




# Chemical leveling mechanism and oxide film properties of additively manufactured Ti–6Al–4V alloy

Yifei Zhang<sup>1,2</sup> , Jianzhong Li<sup>1,2,\*</sup>, Shuanghang Che<sup>1,2</sup>, Zhongdong Yang<sup>1,2</sup>, and Yanwen Tian<sup>1,2</sup>

<sup>1</sup>School of Metallurgy, Northeastern University, Shenyang 110819, China

<sup>2</sup>Liaoning Key Laboratory for Metallurgical Sensors and Technology, Northeastern University, Shenyang 110819, China

Received: 1 April 2019

Accepted: 21 July 2019

Published online:  
29 July 2019

© Springer Science+Business Media, LLC, part of Springer Nature 2019

## ABSTRACT

This paper presents a new approach to modify the surface of the Ti–6Al–4V alloy fabricated by additive manufacturing. This method is particularly suitable for titanium or titanium alloy components with complex shapes (such as pipes, holes and internal flow paths) which are difficult to be polished by conventional methods. The corresponding electrochemical tests were carried out in Hanks' balanced salt solution. The results demonstrated that the chemical polishing of additively manufactured Ti–6Al–4V obtained a high-quality surface through the combination of oxidation corrosive action and polishing liquid flow by reducing the peak-to-valley spacing and smoothing the alloy surface. After chemical polishing, a passivation film consisted of rutile and anatase formed on the alloy surface, which showed n-type semiconductor characteristics and had a lower donor density, leading to the increase in the corrosion resistance.

## Introduction

Additive manufacturing (AM), as an important and fast-growing manufacturing technology, produces metal parts by adding materials layer by layer based on computer-designed 3D solid models. It has been gradually applied in the fields of the aviation industry, biomedical engineering, navigation and construction due to its advantages in build parts with geometric and material complexities. After three decades of development, it has become a mainstream manufacturing process and has been changing the global parts manufacturing and logistics field [1, 2].

Being by far the most reported, Ti–6Al–4V alloy is believed to be a research hotspot and an important material for additive manufacturing technology due to its excellent mechanical properties, chemical properties and processing properties. However, because of the unsuitable energy density in manufacturing process, titanium alloy parts manufactured by laser additive tend to produce voids and unmelted powder defects, resulting in a decrease in surface smoothness [3]. The surface quality of metals has a great influence on its performance and application effect; especially for implanted metal-like medical devices, the surface quality is directly related to its efficacy and complications [4]. Therefore, in practical

Address correspondence to E-mail: lijz@smm.neu.edu.cn

application of titanium and its alloys, it is usually required a surface treatment. It has been demonstrated that the surface polishing is a popular method to improve the surface quality of metals and enhance their performance. A number of surface modification techniques were used to obtain a smooth surface like mechanical polishing, chemical polishing, electrochemical polishing, ultrasonic polishing, laser polishing, liquid jet polishing, etc. [5, 6]. Generally, titanium alloys produced by additive manufacturing have irregular shapes or minute sizes. It is difficult to achieve smooth surface by traditional polishing routes. Hence, the surface modification problem has been receiving much attention [7]. Among them, the chemical polishing is widely used in the surface treatment of materials because of its simple operation, less influencing factors, lower requirements on the shape of the parts and better polishing results.

Chemical polishing is an efficient method which allows reducing the surface roughness of metals through the selectively dissolving of uneven areas on sample surface by chemical etching to eliminate wear marks and achieve leveling effect [8]. The equipment of chemical polishing is simple, and it is capable of handling tiny parts or complex geometric shapes with thin tubes, deep holes, meshes and curved surfaces. Currently, the popular system of chemical polishing solution is mainly composed of nitric acid and its salt series, chromic acid and its salt series and hydrogen peroxide series. Each of the polishing systems has its advantages and disadvantages [9, 10]. The polishing effect of nitric acid is favorable, but the use of nitric acid will produce harmful gases such as nitrogen oxides; this endangers the human body and pollutes the environment [11]. The polishing effect of chromic acid is also satisfying, but hexavalent chromium can cause cancer. Moreover, the removing of hexavalent chromium remained on the parts surface increases the difficulty of polishing process [12]. Although the polishing solution of hydrogen peroxide is environmental friendly, the chemical polishing is an exothermic process; the increase in temperature accelerates the decomposition of hydrogen peroxide, resulting in a poor stability [13]. In terms of chemical polishing for surface treatment of metallic materials, a large number of polishing methods have been researched and applied for titanium and its alloys to obtain a smooth surface with favorable properties.

Hidemasa [14] studied the chemical polishing of titanium dentures using  $\text{HNO}_3/\text{HF}$  solution and

found that the accuracy, surface roughness, surface structure and stability of titanium buckle were remarkably enhanced when polished for 1–5 min. Zhang and Shi [15] developed a new environment-friendly slurry for chemical–mechanical polishing of titanium alloys using a polishing solution consisting of silica, hydrogen peroxide, malic acid and deionized water. The surface roughness  $R_a$  obtained was lower comparable to the previously reported Ti alloy. Łyczkowska [16] researched a chemical surface treatment of Ti–6Al–7Nb alloy with complex spatial structures prepared by powder-bed selective laser melting and observed that the chemical polishing improved the surface quality of Ti–6Al–7Nb as well as removed loose powder particles trapped in the porous structure. Kaushik [17] sought to develop a green approach using a solution of emulsifiable oil and hydrogen peroxide for chemical–mechanical polishing of Ti alloy instead of toxic and hazardous chemicals.

With an increasing demand of industrial practice, the efficient environment-friendly process has become a focus of alloy post-treatment and is widely used for surface polishing. In addition, scholars have reported that the chemical polishing of titanium alloy led to the formation of a protective oxide film on the alloy surface, which was essential for alloy properties [18]. Generally, the chemical polishing obtains a smooth surface with low roughness by one-step process. However, a few reports stated that a two-step chemical polishing obtains a preferable surface with organized nanostructures and achieves a desired performance comparable to those of alloys processed through one-step polishing [19].

Although the chemical polishing of titanium alloys has been becoming mature and formed two mainstream viewpoints based on the mucosal theory and passive film theory, scholars principally pay attention to the process parameters of chemical polishing and polishing effects. No report is available on the role of each component in a chemical solution, and no consensus precise mechanism of chemical polishing has been well elucidated yet. Demands for efficient polishing of titanium alloys and controllable preparation of oxide films are still urgent [20]. Therefore, in this paper, smoothing process of Ti–6Al–4V alloys prepared by additive manufacturing in course of the chemical polishing was systematically analyzed from the aspects of morphology, composition and roughness. The corrosion resistance of specimens in body

fluid environment was improved by homogenizing alloy structures and components through a two-step chemical process. These results provide a theoretical basis for optimizing the surface quality of additively manufactured Ti–6Al–4V alloy, especially for complex workpieces, such as pipes, holes and internal flow paths, and offering better conditions for controllable preparation of protective oxide films on the alloy substrate and are vital to increase the corrosion resistance of Ti–6Al–4V alloy.

## Materials and methods

### Materials and pretreatment

Additively manufactured Ti–6Al–4V alloy was selected as the experimental material, and the compositions of Ti–6Al–4V alloy in weight were 0.018% N, 0.036% C, 0.2% O, 0.003% H, 1.78% Fe, 6.4% Al, 4.08% V and balance Ti. The obtained Ti–6Al–4V specimen was cut into small pieces with a thickness of 2 mm and a diameter of 15 mm. Chemical solutions used in this paper were configured by analytical grade reagent; the compositions are as follows:

Solution  $G_1$ —containing 2.81–2.98 mol L<sup>-1</sup> ammonium hydrogen fluoride, 11.96–12.30 mol L<sup>-1</sup> hydrogen peroxide, 0.43–0.50 mol L<sup>-1</sup> hexamethylenetetramine and 8.11–8.34 mol L<sup>-1</sup> nitric acid.

Solution  $G_2$ —containing 5.25–5.75 mol L<sup>-1</sup> sodium dihydrogen phosphate, 0.24–0.29 mol L<sup>-1</sup> thiourea, 0.033–0.037 mol L<sup>-1</sup> sodium silicate, 3.82–4.06 mol L<sup>-1</sup> sulfosalicylic acid and 0.005–0.006 mol L<sup>-1</sup> sodium dodecyl sulfate.

Before surface treatment, Ti–6Al–4V alloys were degreased in an acetone ultrasonic bath and rinsed with distilled water.

### Two-step chemical polishing

The chemical polishing process described herein was carried out in two steps: In the first step of polishing, Ti–6Al–4V specimens were placed into a chemical polishing solution  $G_1$  and remained at a temperature of  $30 \pm 0.1$  °C for 10–12 min. The polishing process was accompanied by magnetic stirring; then, the specimens were removed from the solutions, washed with deionized water and blow-dried. In the second step, the specimens were introduced into a chemical polishing solution  $G_2$  and remained at a temperature

of  $65 \pm 0.1$  °C for 80–90 s to perform a leveling and brightening process. After that, the treated specimens were taken out and cleaned ultrasonically and dried. In both polishing steps, weight loss  $w$  of each specimen was recorded using a METTLER electronic analytical balance. The surface roughness  $R_a$  was measured by a MarSurf PS1-M300 roughness tester. The measuring direction was perpendicular to the rolling direction, and the sampling evaluation length was 5.6 mm. To ensure the repeatability of the results, five measurements were conducted on each tested sample.

### Surface analysis and electrochemical tests

Surface morphology of Ti–6Al–4V alloy was assessed by a field-emission scanning electron microscopy (SEM, Quanta FEG 250). Three-dimensional morphological properties of specimens were characterized using an atomic force microscopy (AFM, ESCALAB250). A Raman spectroscopy (CN61 M/LRS-3) was applied to analyze the surface compositions of specimens. A He–Ne laser with an excitation wavelength of 632.8 nm acted as an excitation light. The power was 413 mW, and the Raman spectrum was measured at room temperature.

After chemical polishing, electrochemical characterization of Ti–6Al–4V was evaluated in Hanks' balanced salt solution, which contained 0.137 mol L<sup>-1</sup> NaCl, 0.00417 mol L<sup>-1</sup> NaHCO<sub>3</sub>, 0.00269 mol L<sup>-1</sup> Na<sub>2</sub>HPO<sub>4</sub>, 0.00049 mol L<sup>-1</sup> MgCl<sub>2</sub>·6H<sub>2</sub>O, 0.00041 mol L<sup>-1</sup> MgSO<sub>4</sub>·7H<sub>2</sub>O, 0.00167 mol L<sup>-1</sup> CaCl<sub>2</sub>, 0.00536 mol L<sup>-1</sup> KCl, 0.0004 mol L<sup>-1</sup> KH<sub>2</sub>PO<sub>4</sub> and 0.0056 mol L<sup>-1</sup> glucose. The pH of the Hanks' solution was adjusted with 1 mol L<sup>-1</sup> HCl to 7.3–7.5 [21]. A PARSTAT 2273 electrochemical workstation and a standard electrochemical cell with three electrodes, a reference electrode (saturated calomel electrode), a counter electrode (platinum electrode) and a working electrode (Ti–6Al–4V specimen), were employed [22]. The exposed area of alloy specimen was approximate to 1 cm<sup>2</sup>. The electrochemical tests were carried out at room temperature ( $25 \text{ °C} \pm 1 \text{ °C}$ ). Prior to measurement, the open circuit of the alloy in Hanks' solution was recorded for 120 min to reach a stable state. The anodic polarization curve of the Ti–6Al–4V alloy was measured by scanning a potential range from  $-1.0$  V to  $0.8$  V (vs. SCE) at a scan rate of  $1 \text{ mV s}^{-1}$ . A high potential sweep rate of  $20 \text{ mV s}^{-1}$  was used in Mott–Schottky measurement from  $-1.8$  to  $1.8$  V in order to avoid the polarizing

effect on passive film. The frequency range of the impedance spectrum was measured from 0.01 Hz to 100000 Hz, and the signal amplitude of the sine wave was 10 mV. The test results were fitted by ZSimpWin. For each specimen, at least three independent measurements were performed to ensure reproducibility.

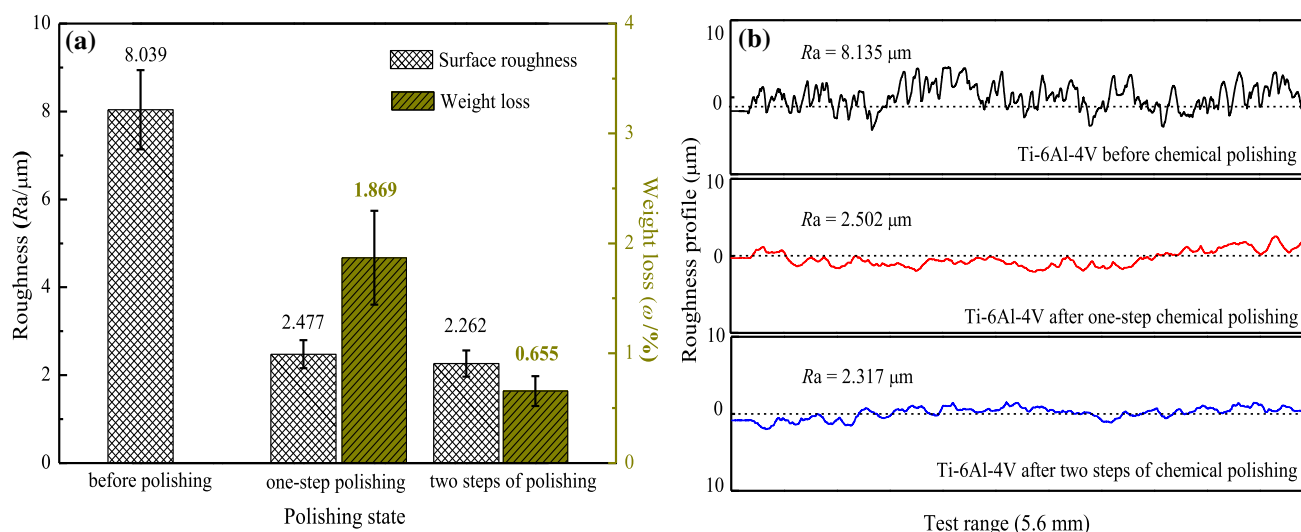
## Results and discussion

### Surface roughness and morphology

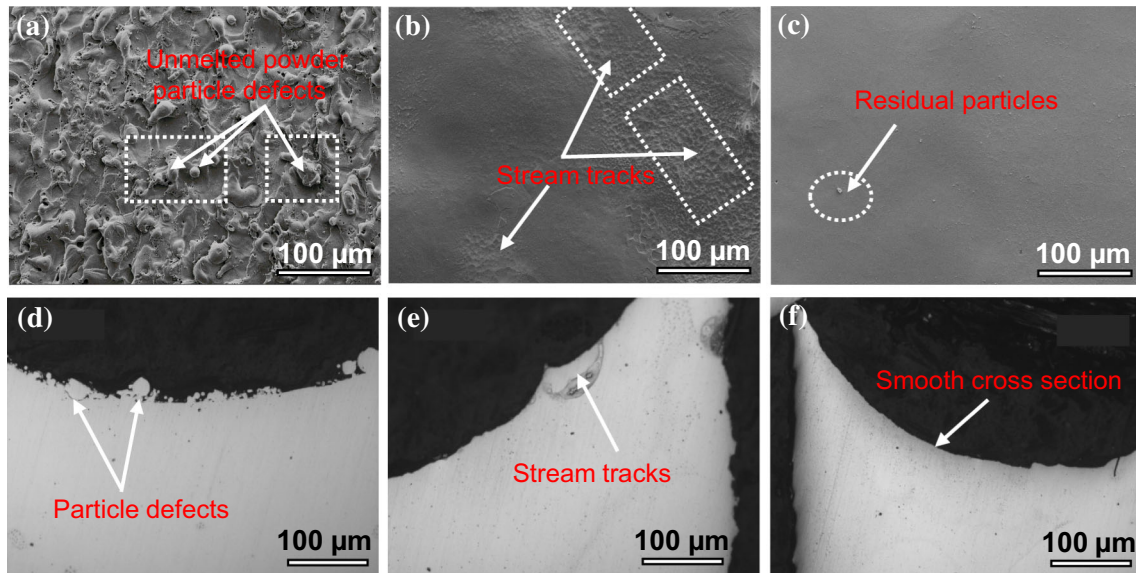
Figure 1a gives the surface roughness and weight loss of Ti-6Al-4V alloy for each step of polishing. The surface roughness  $R_a$  of Ti-6Al-4V specimen before chemical polishing was 8.04  $\mu\text{m}$ . After one-step polishing, the surface roughness was 2.48  $\mu\text{m}$ , which decreased 2.5–3.5 times regarding the surface roughness obtained from the unpolished specimen, and the weight loss of the sample was 1.87%. On the basis of the first polishing step, the surface roughness of Ti-6Al-4V decreased to 2.26  $\mu\text{m}$  after two steps of polishing, which was further decreased by 8.68%. The weight loss of the specimen was 0.66%. Corresponding surface roughness profiles of Ti-6Al-4V alloys are shown in Fig. 1b. As can be seen from Fig. 1, the chemical polishing effectively decreased the surface roughness of Ti-6Al-4V, after polishing the fluctuation of the roughness profile gradually decreased, and the specimen was smoothed. Furthermore, it can be inferred in conjunction with

Fig. 1a and b that in the first step of polishing, the roughness variation and weight loss of the specimen were large and a macro-smoothing took place. However, in the second step of polishing, the indexes of the specimen changed little. The surface roughness decreased gradually under the condition of small weight loss. A microscopic smoothing occurred principally. This demonstrated that a two-step chemical polishing can decrease the surface roughness and improve the surface appearance of additively manufactured Ti-6Al-4V effectively.

In order to observe the surface morphologies of the Ti-6Al-4V intuitively and analyze the polishing effect, surface morphologies and corresponding cross-sectional morphologies of Ti-6Al-4V specimens are characterized, as shown in Fig. 2. From the SEM observations in Fig. 2, it can be clearly seen that the chemical polishing significantly decreased the surface roughness of Ti-6Al-4V alloys. Prior to chemical polishing, the specimen surface observed was rough and uneven with a large amount of unmelted powder particle defects (Fig. 2a and d) [23]. After the first step of polishing, phase particles adhering to the alloy surface were peeled off and a few stream tracks were detected. The surface roughness of the specimen decreased visibly (Fig. 2b and e). While after the second step of polishing, the specimen surface further smoothed and the stream tracks disappeared. The smoothing effect attained a relatively high level, and a leveled and shiny surface was obtained (Fig. 2c and f).



**Figure 1** Sample characteristics of Ti-6Al-4V alloy before and after chemical polishing. **a** Surface roughness and weight loss of Ti-6Al-4V alloy. **b** Surface roughness profile of Ti-6Al-4V alloy.



**Figure 2** Surface and cross-sectional morphologies of tubular Ti-6Al-4V components. **a** Surface morphology of Ti-6Al-4V before chemical polishing. **b** Surface morphology of Ti-6Al-4V after one-step chemical polishing. **c** Surface morphology of Ti-6Al-4V

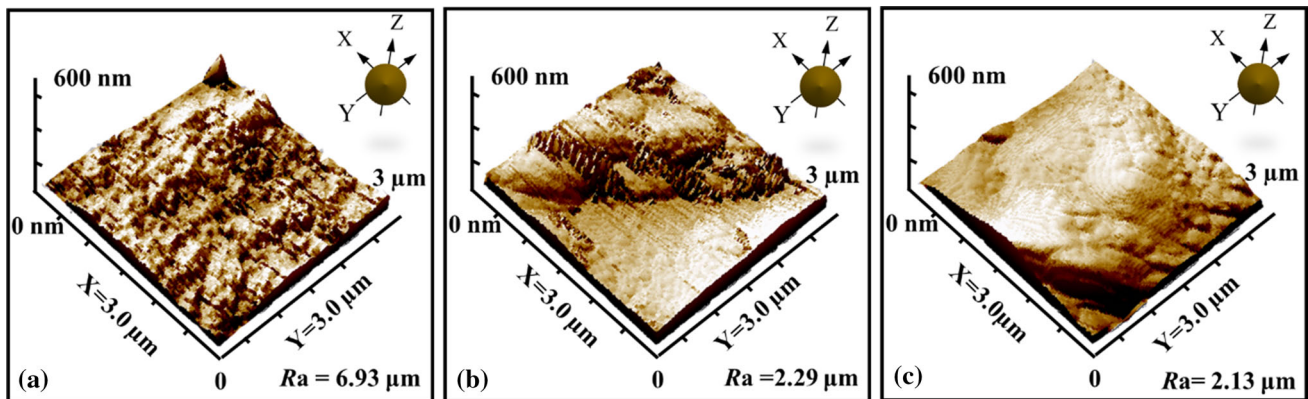
after two steps of chemical polishing. **d** Cross-sectional morphology of Ti-6Al-4V before polishing. **e** Cross section of Ti-6Al-4V after one-step chemical polishing. **f** Cross section of Ti-6Al-4V after two steps of chemical polishing.

The 3D images of  $3 \times 3 \mu\text{m}$  areas, obtained by AFM of the specimens before and after polishing, are observed in Fig. 3, where Fig. 3a shows the specimen before polishing, Fig. 3b plots the specimen surface with the first polishing step, and Fig. 3c gives the 3D images of the sample after two-step polishing process. For additively manufactured Ti-6Al-4V alloy, the first polishing step decreased the surface roughness significantly. In the region investigated in AFM, the higher peaks on the sample surface preferentially dissolved compared to the lower valleys, and the spacings between the peaks and valleys ( $R_p - V$ ) gradually reduced, achieving the leveling of the

sample surface [24]. In the second step, the ( $R_p - V$ ) further decreased, and the overall roughness decreased to  $2.13 \mu\text{m}$ ; thus, the surface of the sample became uniform and bright.

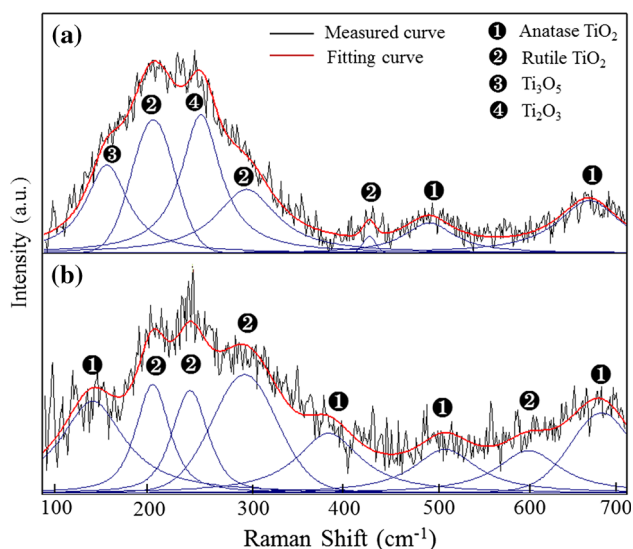
### Surface composition analysis

Figure 4 plots the Raman spectrum of the surface oxide films at different polishing stages. The standard Raman band positions corresponding to each oxide in the spectrum are shown in Table 1. Despite the strong oscillations of the baseline due to the fluorescence response of the edge filter of the Raman



**Figure 3** AFM images of the surface topography of Ti-6Al-4V alloy. **a** Ground specimen before polishing. **b** Well-polished specimen after the first polishing step. **c** Well-polished specimen after two-step polishing process.

spectrum, the characteristic peaks of titanium oxides were still obtained by deconvolution with Gaussian fittings [25]. As shown in Fig. 4, after one or two steps of chemical polishing, compositions of the titanium oxide layer on the sample surface were substantially similar, and the apparent difference is that slightly lower valence oxides were detected after one-step polishing. In the case of Fig. 4a, an obvious peak appearing at  $261\text{ cm}^{-1}$  was ascribed to the vibration of  $\text{Ti}_3\text{O}_5$ , and the band around  $261\text{ cm}^{-1}$  could be corresponding to  $\text{Ti}_2\text{O}_3$ , which exhibited the symmetric bending vibration of Ti–O–Ti. Two clear peaks at  $503$  and  $662\text{ cm}^{-1}$  were identified as anatase  $\text{TiO}_2$ , which was tetragonal with unit cell parameters of  $\alpha = \beta = \gamma = 120^\circ$  and belonged to the space group  $D19\ 4\ h(I4_1/amd)$ . On the other hand, in rutile  $\text{TiO}_2$ , the unit cell parameter was  $\alpha = \beta = \gamma = 90^\circ$  and it belonged to the  $D14\ 4\ h(P4_2/mnm)$  space group [26]. The characteristic bands at  $221$ ,  $299$  and  $435\text{ cm}^{-1}$  indicated the presence of rutile  $\text{TiO}_2$  according to the standard peaks. Figure 4b shows the spectrum of anatase and rutile  $\text{TiO}_2$  in the investigated sample, where four peaks of anatase, located at  $149$ ,  $389$ ,  $514$  and  $675\text{ cm}^{-1}$ , were observed, and the measured Raman peak positions were assigned to the Raman vibration modes of Eg, A1g + B1g, A1g and B1g [27]. Moreover, the bands associated with rutile  $\text{TiO}_2$  presented four peaks at  $213$ ,  $242$ ,  $295$  and  $600\text{ cm}^{-1}$  likewise. Among them, the Raman vibration of



**Figure 4** Raman peak spectrum of titanium alloy surface in chemical polishing processes. **a** Raman spectrum after one-step polishing. **b** Raman spectrum after two steps of polishing.

medium intensity appeared at  $213$  and  $242\text{ cm}^{-1}$  may be due to the swing of titanium–oxygen bond. The vibration frequency of the strong peak at  $295\text{ cm}^{-1}$  was caused by the O–Ti–O symmetric bending vibration mode. At Raman shift of  $600\text{ cm}^{-1}$ , the characteristic peak of rutile belonged to the vibration of O–Ti–O axial antisymmetric stretching-type and equatorial bending vibration. These Raman spectra supported, with a high degree of confidence, the conclusion that after chemical polishing, the oxide layer on the alloy surface was mainly  $\text{TiO}_2$ , which was comparable to the results obtained from Ti–6Al–4V specimen after electrochemical polishing [28].

### Electrochemistry property analysis

Polarization curves of Ti–6Al–4V alloys in Hanks' solution are shown in Fig. 5. The sample before chemical polishing was characterized by a corrosion potential of  $-0.43\text{ V}$ , and a passivation plateau appeared at higher anodic potentials of more than  $3.66\text{ V}$ . After chemical polishing, the corrosion potential of Ti–6Al–4V shifted to the anodic direction and the alloy seemed to display a higher corrosion potential, which implied a stronger thermodynamic stability.

At voltages far from  $E_{\text{corr}}$ , the current density reflects the kinetics of the reaction that predominates in this region. Slopes of the anode and cathode in Tafel region are represented by  $\beta_a$  and  $\beta_c$ ; when  $E \gg E_{\text{corr}}$ , the anodic curve slope  $\beta_a$  in the Tafel region can be expressed by the equation [29]

$$\beta_a = \left( \frac{dE}{d \log i} \right)_{E \gg E_{\text{corr}}} = \frac{-2.3RT}{\delta_a MF}, \quad (1)$$

while when  $E \ll E_{\text{corr}}$ , the cathode slope  $\beta_c$  is given by the expression:

$$\beta_c = \left( \frac{dE}{d \log i} \right)_{E \ll E_{\text{corr}}} = \frac{-2.3RT}{\delta_c MF} \quad (2)$$

where  $E$  is the applied voltage,  $i$  is the measured current density,  $\delta_a$  and  $\delta_c$  are the charge transfer coefficients for the anodic and cathode reactions,  $R$  is the gas constant,  $T$  is the absolute temperature,  $M$  is the metal valence and  $F$  is the Faraday constant.

Electrochemical parameters of Ti–6Al–4V alloy at different polishing steps are listed in Table 2; it can be seen that with chemical polishing proceeding, the corrosion current changed. The current density at sample after one-step chemical polishing was about

**Table 1** Raman peak positions of Ti-6Al-4V alloy at different chemical polishing steps

Polishing status	Raman band (cm <sup>-1</sup> )											
	Anatase				Rutile				Ti <sub>3</sub> O <sub>5</sub>	Ti <sub>2</sub> O <sub>3</sub>		
Standard	145	398	515	656	218	238	294	448	608	155	265	
One step			503	662	221		299	435		163	261	
Two steps	149	389	514	675	213	242	295		600			

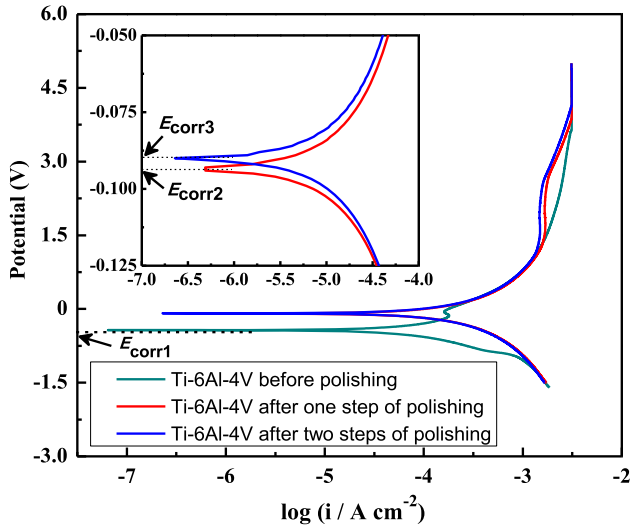


**Figure 5** Polarization curves in Hanks' solution for unpolished Ti-6Al-4V and Ti-6Al-4V polished for one or two steps.

1.46 mA cm<sup>-2</sup>, and that at sample after two steps of polishing was appropriately 1.37 mA cm<sup>-2</sup>. Although the corrosion rate is proportional to the anode current density under active conditions, the passive state in oxidizing conditions is not negligible for the evaluation of the corrosion resistance of Ti-6Al-4V alloys. It is noticed that the activation region was not observed in a wide potential range from 1.38 to 2.54 V, which suggested that a steady passive behavior can be identified over this potential range after chemical polishing. With chemical polishing proceeding, the passivation current density decreased in a sequential order: unpolished sample (0.100 mA cm<sup>-2</sup>) > one step of chemical polishing (0.053 mA cm<sup>-2</sup>) > two steps of chemical polishing (0.047 mA cm<sup>-2</sup>). This supported the analysis in corrosion potential. Therefore, based on the above

**Table 2** Electrochemical parameters of Ti-6Al-4V alloy at different polishing steps

Sample	E <sub>corr</sub> (V)	i <sub>corr</sub> (μA cm <sup>-2</sup> )	b <sub>a</sub> (mV dec <sup>-1</sup> )	-b <sub>c</sub> (mV dec <sup>-1</sup> )	i <sub>pass</sub> (mA cm <sup>-2</sup> )
Unpolished	- 0.433	54.51	4.823	5.321	0.100
One step	- 0.095	1.46	4.916	4.865	0.053
Two steps	- 0.089	1.37	4.975	4.833	0.047

analysis, the measured polarization curves indicated that the chemical polishing can afford better corrosion protection to the alloy substrates.

AC impedance characteristics of the surface oxide films on Ti-6Al-4V alloys were measured, which are plotted in Fig. 6. As seen in Fig. 6a, all the Nyquist curves were featured with two semicircles. The chemical polishing did not change the feature of the Nyquist plots, but the radius of the capacitor arcs increased as the polishing process progressed. After chemical polishing, the Ti-6Al-4V presented a higher impedance modulus in the low-frequency region, and the frequency negative phase angle increased, indicating that the corrosion was weakened. The Bode phase diagrams depicted two time constants which were generally considered to be the response of a non-homogeneous film caused by a two-layer structure on the sample surface [30, 31]. The inner barrier layer controlled the impedance spectrum at high and intermediate frequencies, while the outer layer dominated the low frequencies [32]. The equivalent circuits used for fitting the EIS data are shown in Fig. 6d, which shows that the oxide film has a structural feature composed of a dense inner layer (barrier layer) and a porous outer layer. Corresponding fitting results are shown in Table 3. In the proposed model, R<sub>s</sub> is the solution resistance and C<sub>1</sub>, R<sub>1</sub> and C<sub>2</sub>, R<sub>2</sub> correspond to the capacitance and resistance of the outer layer and inner layer, respectively. The impedance of a constant phase element (CPE) is defined as Z<sub>CPE</sub>

$$Z_{CPE} = [Y(j\omega)^a]^{-1} \tag{3}$$

where Y is the constant of CPE, expressed in F cm<sup>2</sup> s<sup>(n-1)</sup>; j is the imaginary number; ω represents the

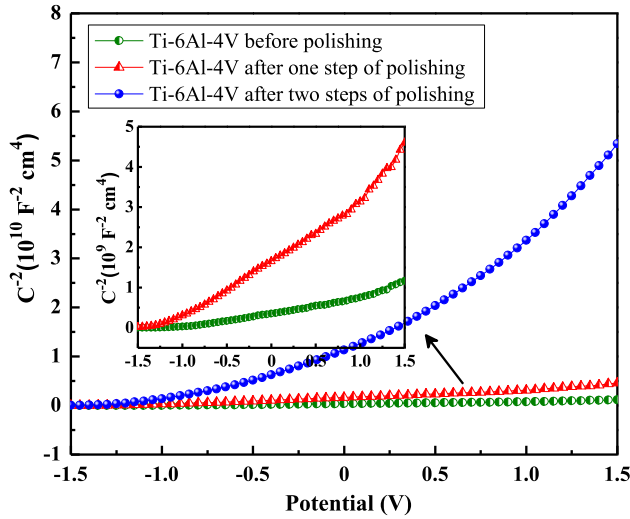


**Figure 6** Mott–Schottky plots of the Ti–6Al–4V alloys in Hanks’ solution.

angular frequency;  $\alpha$  is defined as the diffusion coefficient and  $-1 \leq \alpha \leq 1$ . When  $\alpha = 1$ , the CPE describes an ideal capacitor; when  $0.5 < \alpha < 1$ , it indicates a different frequency dispersion due to local inhomogeneities in the dielectric material [33]. Then, the non-ideal capacitance caused by the surface roughness or unevenness of the electrode in Fig. 6d can be converted into a pure capacitance  $C$  by Eqs. (4) and (5) [34, 35]

$$C_1 = Q_1^{1/\alpha_1} (R_s^{-1} + R_1^{-1})^{\alpha_1 - 1/\alpha_1} \quad (4)$$

$$C_2 = (Q_2 R_2)^{1/\alpha_2} / R_2 \quad (5)$$

where  $Q = Z_{CPE}$  [Eq. (3)].

The observed lower solution resistance ( $R_s$ ) was mainly due to the presence of a large amount of ions in the Hanks’ solution. The value of  $\alpha_1$  decreased after polishing, indicating that the chemical polishing decreased defects and pores on the formed film [36]. As regards the parameters of the inner oxide film, Table 3 shows that both  $\alpha_2$  and  $R_2$  increased after chemical polishing, suggesting that the chemical polishing modified the films formed on the Ti–6Al–4V, enhancing the barrier function of the inner layer,

reducing the number of defects and increasing the corrosion resistance [37]. Therefore, the comprehensive analysis suggests that the chemical compositions and microstructures on the surface of the chemical-polished sample have a direct impact on its electrochemical performance. Compared to the unpolished alloy, the change in surface roughness, compositions and structure of the polished sample results in an increase in corrosion resistance.

Since the oxide film on the surface of the Ti–6Al–4V after polishing can be regarded as a dielectric plate capacitor, the thickness of the oxide film ( $d$ ) is closely related to its capacitance value and can be expressed by Eq. (4) [38]

$$d = S \epsilon \epsilon_0 \frac{1}{C_{dp}} \quad (6)$$

where  $S$  is the electrode area, taken as  $1 \text{ cm}^{-2}$ ;  $\epsilon$  and  $\epsilon_0$  are the dielectric constants of the oxide film and the vacuum, taken as  $56 \text{ F cm}^{-1}$  and  $8.854 \times 10^{-12} \text{ F cm}^{-1}$ , respectively.  $C_{dp}$  stands for the capacitor of the passivation film. It is clear that the thickness of the oxide film on the alloy surface is negatively correlated with the capacitance value, that is, the capacitance value of the passivation film can simply estimate the thickness of the oxide film [39]. As can be calculated from the data in Table 3, the passive films in the samples before and after polishing were about  $0.590 \text{ }\mu\text{m}$ ,  $0.378 \text{ }\mu\text{m}$  and  $0.192 \text{ }\mu\text{m}$ , implying that after chemical polishing, the thickness of the oxide films decreased and the conductivity of the electrode was weakened, resulting in an increase in corrosion resistance.

There are some relationships between the semi-conducting properties and the corrosion resistance of the passive film. These properties can be determined by analyzing the curve of capacitance as a function of the electrode potential, which reflects the charge distribution in the passive film. When the oxide film is in contact with the solution interface, the semiconductor oxide film and the solution carry opposite charges, respectively [40]. The excess charge of the semiconductor film is distributed in the space charge

**Table 3** Impedance parameters of Ti–6Al–4V alloy after different steps of chemical polishing

Polishing status	$R_s$ ( $\Omega \text{ cm}^2$ )	$C_1$ ( $\text{F cm}^{-2}$ )	$\alpha_1$	$R_1$ ( $\Omega \text{ cm}^2$ )	$C_2$ ( $\text{F cm}^{-2}$ )	$\alpha_2$	$R_2$ ( $\Omega \text{ cm}^2$ )	$\chi^2$ ( $\times 10^{-3}$ )
Unpolished	1.47	$2.74 \times 10^{-4}$	0.80	16.05	$0.84 \times 10^{-5}$	0.69	18.56	0.17
After one step	1.99	$3.23 \times 10^{-5}$	0.93	19.64	$1.31 \times 10^{-5}$	0.58	155.60	2.83
After two steps	1.86	$2.16 \times 10^{-5}$	0.89	12.88	$2.58 \times 10^{-5}$	0.69	228.20	2.25



**Table 4** Solution system formulation and the function of each chemical reagent

Chemical reagent	Component role	Main effect	Chemical reagent	Component role	Main effect
Ammonium hydrogen fluoride	Corrodent	Erosion effect	Thiourea	Reaction accelerator/metal rust inhibitor	Promote reaction and prevent metal rust
Hydrogen peroxide	Oxidant	Oxidation effect	Sodium silicate	Brightener/defoamer	Improve polishing quality
Nitric acid	Corrodent	Erosion effect	Sulfosalicylic acid	Corrodent	Corrosion stripping effect
Hexamethylenetetramine	Inhibiter	Control reaction rate	Sodium dodecyl sulfate	Surfactant	Promote adsorption and desorption, increase surface activity
Sodium dihydrogen phosphate	Conditioning agent	Adjusting solution environment			

layer. When the space charge layer shows a depletion layer, the relationship between the space charge capacitance ( $C$ ) and potential ( $E$ ) can be analyzed using the Mott–Schottky equation [41].

$$\frac{1}{C^2} = \frac{2}{\epsilon\epsilon_0eN_d} \left( E - E_{fb} - \frac{kT}{e} \right) \tag{7}$$

for  $n$  - type semiconductor

$$\frac{1}{C^2} = -\frac{2}{\epsilon\epsilon_0eN_a} \left( E - E_{fb} - \frac{kT}{e} \right) \tag{8}$$

for  $p$  - type semiconductor

where  $C$  is the capacitance of the space charge layer of the oxide film;  $N_d$  is the donor density;  $N_a$  is the acceptor density;  $E$  is the electrode potential;  $E_{fb}$  is the flat band potential;  $\epsilon_0$  is the vacuum permittivity with a value of  $8.854 \times 10^{-12}$  F cm<sup>-1</sup>, and  $\epsilon$  stands for the dielectric constant of the passive film and usually the value range for titanium is from 48 to 110, taken as 56 F cm<sup>-1</sup> in this article. The electronic charge of  $1.602 \times 10^{-19}$  C is expressed as  $e$ , and the Boltzmann constant and absolute temperature are represented by  $K$  and  $T$ , respectively. When the temperature is a normal temperature, the value of  $kT/e$  is about 25 mV, which could be neglected.

Mott–Schottky curves of the passivation films formed on the surface of Ti–6Al–4V alloys before and after chemical polishing are shown in Fig. 7. It is seen that all the passive films formed on the surface of Ti–6Al–4V showed an n-type semiconductor behavior with positive slopes. Moreover, the slope of Mott–Schottky curves increased with the proceeding of chemical polishing. It is acknowledged that that the passive film stability is affected by the concentration of the donor/acceptor concentration and the diffusion coefficient [42]. Compared with Ti<sup>n+</sup> interstitial, the oxygen vacancy has lower formation energy [43]. Therefore, for the n-type semiconductor passive film formed on the surface of Ti–6Al–4V, the main donors were oxygen vacancies ( $V_2 + O$ ). Due to the enrichment of oxygen vacancies, higher donor density was detrimental to the passivation layer. The presence of oxygen vacancies can increase the affinity of the oxide film for aggressive ions [44]. According to Eq. (7), the donor density  $N_d$  can be calculated from the slope of Mott–Schottky plots and it is inversely proportional to the slope value. The obtained donor density of the passive film before polishing was  $6.22 \times 10^{19}$  cm<sup>-3</sup>, and the passivation film after one-step and two-step chemical polishing had a donor

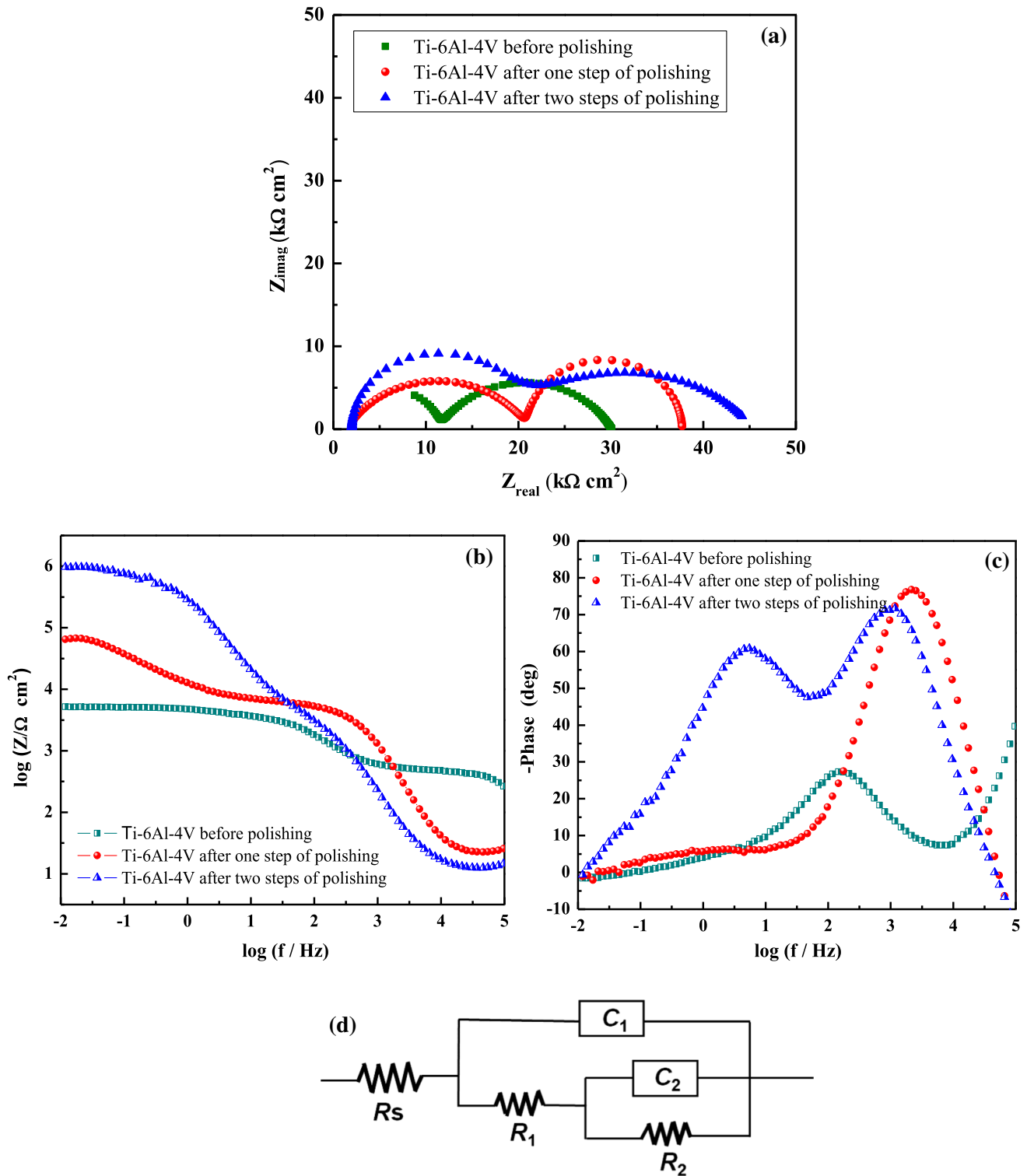


**Figure 7** Data for electrochemical impedance spectroscopy. **a** Nyquist plots of Ti-6Al-4V. **b** Bode modulus plots of Ti-6Al-4V. **c** Bode phase plots of Ti-6Al-4V. **d** Equivalent circuit used for fitting EIS data.

density of  $7.75 \times 10^{18}\text{ cm}^{-3}$  and  $2.05 \times 10^{18}\text{ cm}^{-3}$ , respectively. The decrease in donor density indicated a decrease in carrier concentration in the passivation

film, that is, a decrease in the concentration of oxygen vacancies, indicating that the passivation films after

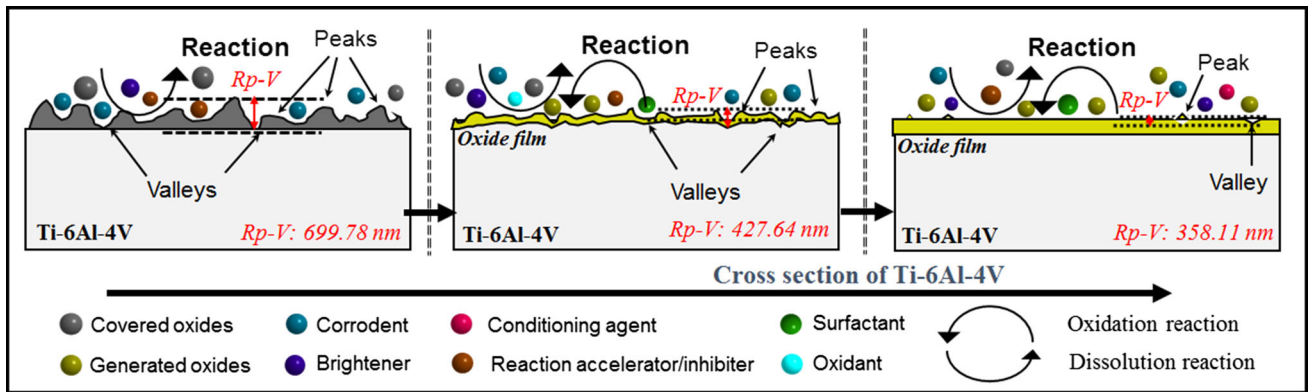


**Figure 8** Leveling mechanism of Ti-6Al-4V alloy during chemical polishing process.

chemical polishing had a relatively weaker affinity for the aggressive ion  $\text{Cl}^-$ .

### Leveling mechanism of chemical polishing

The chemical polishing of Ti-6Al-4V alloy is complicated. The entire polishing process relies on two simultaneous but opposite reactions, and the reaction and diffusion phenomena at the metal/solution interface control the polishing process. One of the complex processes is a dissolution reaction, in which the metal enters the solution in the form of ions; and the other is an oxidation reaction, in which an oxide layer forms on the surface of the alloy. The formed oxide layer is protective to a certain extent, limiting the progress of the first reaction. The two opposite reactions compete with each other, resulting in a self-limiting chemical corrosion, achieving a polishing result.

Under the erosion action of corrosive agents such as ammonium hydrogen fluoride, hydrogen peroxide and nitric acid, the oxide film spontaneously formed on the Ti-6Al-4V alloy (mainly  $\text{TiO}_2$  and a small amount of  $\text{TiO}$ ,  $\text{Ti}_2\text{O}_3$  [45]) was peeled off from the sample surface. Then, the oxidation occurred again on the surface of the specimen to form a new layer of more stable and dense oxides. During the reaction, the dissolution rate of the protruding part on the alloy surface was different from the concave portion, which makes the sample reaching a polishing effect gradually (Table 4). Broadly speaking, the polishing process includes the oxide dissolution on the alloy surface, the migration evolution of the oxygen and the formation of a passivation oxide layer [46]. In the polishing solution described above, the oxidation reaction dominates the complex process during the

dissolution and passivation of titanium alloys [47], leading to the formation of a passivation layer with higher valence states; the proceeding reactions can be expressed as:

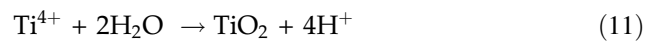
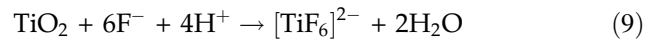


Figure 8 shows the flattening mechanism of Ti-6Al-4V alloy in the chemical polishing. Prior to chemical polishing, the original surface of Ti-6Al-4V alloys had large peak-to-valley spacing and the sample was rough and matte. Under the corrosion action of aggressive components in the polishing solution, higher surface peaks on the alloy surface dissolved preferentially, and lower valleys dissolved later. The distance between the peaks and valleys on the sample surface decreased continuously, achieving a macroscopic polishing or smoothing effect. Under the action of the leveling solution, a micro-smoothing process takes place on the basis of the macroscopic smoothness, which further decreased the surface roughness, increased the surface gloss and improved the appearance. In summary, the first step of chemical polishing is the polishing process, which causes the uneven alloy surface to be flattened at different rates through decreasing the spacing between the peaks and the valleys. The second stage is a smoothing process, which is main to obtain a smooth and shiny surface by flattening the alloy surface and enhancing the sample glossiness. The two-step chemical polishing optimizes the surface treatment of Ti-6Al-4V alloy and obtains a smooth sample, overall. This behavior and mechanism are similar to that observed by Sepúlveda in two-step electropolishing

of aluminum alloys [48], which significantly improves the surface appearance and glossiness of aluminum alloys.

## Conclusions

In this article, an optimized two-step chemical polishing based on the additively manufactured Ti–6Al–4V alloy was studied, and a preferable surface was obtained. The two-step chemical treatment decreased the surface roughness of the Ti–6Al–4V by the erosion action of a polishing solution and then further smoothed the sample surface by using a leveling solution. After polishing, the weight loss rate of the Ti–6Al–4V was merely 2.51%; however, the surface roughness of the sample decreased by 71.86%, achieving a significant improvement in the surface quality of the Ti–6Al–4V. A uniform and stable TiO<sub>2</sub> passivation film with anatase and rutile as the main components formed on the alloy surface. Compared with the unpolished Ti–6Al–4V, the thickness of the passive film on the polished sample surface decreased and the resistance of the passive film increased, resulting in high corrosion resistance.

## Acknowledgements

This work was supported by the Iron and Steel Joint Research Found of National Natural Science Foundation and China Baowu Steel Group Corporation Limited (Grant Number U1760118); and the National Natural Science Foundation of China (Grant Number 51374053).

## References

- [1] Frazier WE (2014) Metal additive manufacturing: a review. *J Mater Eng Perform* 23:1917–1928
- [2] Melchels FPW, Domingos MAN, Klein TJ, Malda J, Bartolo PJ, Huttmacher DW (2012) Additive manufacturing of tissues and organs. *Prog Polym Sci* 37:1079–1104
- [3] Gong HJ, Rafi K, Gu HF, Ram GDJ, Starr T, Stucker B (2015) Influence of defects on mechanical properties of Ti–6Al–4V components produced by selective laser melting and electron beam melting. *Mater Des* 86:545–554
- [4] Zhao BJ, Wang H, Qiao N, Wang C, Hu M (2017) Corrosion resistance characteristics of a Ti–6Al–4V alloy scaffold that is fabricated by electron beam melting. *Mater Sci Eng, C* 70:832–841
- [5] Browne M, Gregson PJ (1994) Surface modification of titanium alloy implants. *Biomater* 15:894–898
- [6] Rie KT, Lampe T (1985) Thermochemical surface treatment of titanium and titanium alloy Ti–6Al–4V by low energy nitrogen ion bombardment. *Mater Sci Eng* 69:473–481
- [7] Gong XJ, Cui YJ, Wei DX, Liu B, Liu RP, Nie Y, Li YP (2017) Building direction dependence of corrosion resistance property of Ti–6Al–4V alloy fabricated by electron beam melting. *Corros Sci* 127:101–109
- [8] Liu XY, Chu PK, Ding CX (2004) Surface modification of titanium, titanium alloys, and related materials for biomedical applications. *Mater Sci Eng* 47:49–121
- [9] Szymczyk P, Junka A, Ziółkowski G, Bartoszewicz M, Chlebus E (2013) The ability of *S. aureus* to form biofilm on the Ti–6Al–7Nb scaffolds produced by selective laser melting and subjected to the different types of surface modifications. *Acta Bioeng Biomech* 15:69–76
- [10] Zhang L, Yuan AM, Qi ZJ, Cai QH, Cheng ZC, Qi H (2018) CFD-based study of the abrasive flow characteristics within constrained flow passage in polishing of complex titanium alloy surfaces. *Powder Technol* 333:209–218
- [11] Nagano H, Kajimura H, Yamanaka K (1995) Corrosion resistance of zirconium and zirconium-titanium alloy in hot nitric acid. *Mater Sci Eng, A* 198:127–134
- [12] Shah UH, Rahman Z, Deen KM, Asgar H, Shabib I, Haider W (2017) Investigation of the formation mechanism of titanium oxide nanotubes and its electrochemical evaluation. *J Appl Electrochem* 47:1147–1159
- [13] Ozdemir Z, Ozdemir A, Basim GB (2016) Application of chemical mechanical polishing process on titanium based implants. *Mater Sci Eng C* 68:383–396
- [14] Shimpo H (2008) Effect of arm design and chemical polishing on retentive force of cast titanium alloy clasps. *J Prosthodont* 17:300–307
- [15] Zhang ZY, Shi ZF, Dua YF, Yu ZJ, Li C, Guo DM (2018) A novel approach of chemical mechanical polishing for a titanium alloy using an environment-friendly slurry. *Appl Surf Sci* 427:409–415
- [16] Łyczkowska E, Szymczyk P, Dybała B, Chlebus E (2014) Chemical polishing of scaffolds made of Ti–6Al–7Nb alloy by additive manufacturing. *Arch Civil Mech Eng* 14:586–594
- [17] Kaushik RM, Bhandakkar AB, Patro TU (2014) Solution of emulsifiable oil and hydrogen peroxide for chemical-mechanical polishing of Ti alloy-A green approach. *Mater Lett* 122:252–255

- [18] Cheng T, Chen Y, Nie X (2013) Surface morphology manipulation and wear property of bioceramic oxide coatings on titanium alloy. *Surf Coat Technol* 215:253–259
- [19] Advincula MC, Petersen D, Rahemtulla F, Advincula R, Lemons JE (2007) Surface analysis and biocorrosion properties of nanostructured surface sol-gel coatings on Ti–6Al–4V titanium alloy implants. *J Biomed Mater Res B Appl Biomater* 80:107–120
- [20] Tomashov ND, Chernova GP, Ruscol YS, Ayuyan GA (1997) The passivation of alloys on titanium bases. *Electrochim Acta* 19:159–172
- [21] Mohan L, Anandan C, Grips VKW (2012) Corrosion behavior of titanium alloy Beta-21S coated with diamond like carbon in Hank's solution. *Appl Surf Sci* 258:6331–6340
- [22] Klein N, Yarnitzky C (1980) Conductometric determination of the uncompensated resistance in a three-electrode system. *Anal Chem* 52:998–999
- [23] Kwon Y, Kim H, Lee S, Chin I, Seong T, Lee W, Lee C (2012) Enhanced ethanol sensing properties of TiO<sub>2</sub> nanotube sensors. *Sens Actuators, B* 173:441–446
- [24] Asgari V, Noormohammadi M, Ramazania A, Kashi MA (2018) A new approach to electropolishing of pure Ti foil in acidic solution at room temperature for the formation of ordered and long TiO<sub>2</sub> nanotube arrays. *Corros Sci* 136:38–46
- [25] Bonu V, Das A, Sivadasan AK, Tyagi AK, Dhara S (2015) Invoking forbidden modes in SnO<sub>2</sub> nanoparticles using tip enhanced Raman spectroscopy. *J Raman Spectrosc* 49:1037–1040
- [26] Regonini D, Jaroenworarluck A, Stevensa R, Bowena CR (2010) Effect of heat treatment on the properties and structure of TiO<sub>2</sub> nanotubes: phase composition and chemical composition. *Surf Interface Anal* 42:139–144
- [27] Ohsaka T, Izumi F, Fujiki Y (1978) Raman spectrum of anatase, TiO<sub>2</sub>. *J Raman Spectrosc* 7:321–324
- [28] Zhang YF, Li JZ, Che SH (2018) Electropolishing mechanism of Ti–6Al–4V alloy fabricated by selective laser melting. *Int J Electrochem Sci* 13:4792–4807
- [29] Dzhurinskiy D, Gaob Y, Yeung WK, Strumban E, Leshchinsky V (2015) Characterization and corrosion evaluation of TiO<sub>2</sub>: n-HA coatings on titanium alloy formed by plasma electrolytic oxidation. *Surf Coat Technol* 269:258–265
- [30] Rammelt U, Reinhard G (1990) On the applicability of a constant phase element (CPE) to the estimation of roughness of solid metal electrodes. *Electrochim Acta* 35:1045–1049
- [31] Adam S, Elzbieta F (2018) Determination of accurate electrode contribution during voltammetry scan of electrochemical capacitors. *J Solid State Electrochem* 22:2135–2139
- [32] Heakal FE, Ghoneim AA, Mogoda AS, Awad KH (2011) Electrochemical behavior of Ti–6Al–4V alloy and Ti in azide and halide solutions. *Corros Sci* 53:2728–2737
- [33] López MF, Gutierrez A, Jimenez JA (2002) In vitro corrosion behaviour of titanium alloys without vanadium. *Electrochim Acta* 47:1359–1364
- [34] Hirschorn B, Orazem ME, Tribollet B, Vivier V, Frateur I, Musiani M (2010) Determination of effective capacitance and film thickness from constant-phase-element parameters. *Electrochim Acta* 55:6218–6227
- [35] Brug GJ, Eeden ALG, Sluyters-Rehbach M, Sluyters JH (1984) The analysis of electrode impedances complicated by the presence of a constant phase element. *J Electroanal Chem Interfacial Electrochem* 176:275–295
- [36] Yang I, Kim SG, Kwon SH, Kim MS, Jung JC (2017) Relationships between pore size and charge transfer resistance of carbon aerogels for organic electric double-layer capacitor electrodes. *Electrochim Acta* 223:21–30
- [37] Liu JH, Yu Q, Yu M, Li SM, Zhao K, Xue B, Zu H (2018) Silane modification of titanium dioxide-decorated graphene oxide nanocomposite for enhancing anticorrosion performance of epoxy coatings on AA-2024. *J Alloys Compd* 774:728–739
- [38] Ismail KM, Fathy AM, Badawy WA (2004) The influence of Ni content on the stability of copper–nickel alloys in alkaline sulphate solutions. *J Appl Electrochem* 34:823–883
- [39] Brunette DM, Tengvall P, Textor M, Thomsen P (2001) Properties and biological significance of natural oxide films on titanium and its alloys. Springer, Berlin
- [40] Hayre RO, Nanu M, Schoonman J, Goossens A (2007) Mott – Schottky and charge-transport analysis of nanoporous titanium dioxide films in air. *J Phys Chem C* 111:4809–4814
- [41] Zhang GA, Cheng YF (2009) Micro-electrochemical characterization and Mott–Schottky analysis of corrosion of welded X70 pipeline steel in carbonate/bicarbonate solution. *Electrochim Acta* 55:316–324
- [42] Ahn SJ, Kwon HS (2004) Effects of solution temperature on electronic properties of passive film formed on Fe in pH 8.5 borate buffer solution. *Electrochim Acta* 49:3347–3353
- [43] Sanchez-Tovar R, Fernandez-Domene RM, García-García DM, García-Anton J (2015) Enhancement of photoelectrochemical activity for water splitting by controlling hydrodynamic conditions on titanium anodization. *J Power Sources* 286:224–231
- [44] Ainouche L, Hamadou L, Kadri A, Benbrahim N, Bradai D (2014) Interfacial barrier layer properties of three generations of TiO<sub>2</sub> nanotube arrays. *Electrochim Acta* 133:597–609

- [45] Babilas D, Urbnczyka E, Sowa M, Maciej A, Korotin DM (2016) On the electropolishing and anodic oxidation of Ti–15Mo alloy. *Electrochim Acta* 205:256–265
- [46] Sowa W, Greń K, Kukharenko AI, Korotin DM, Michalska J (2014) Influence of electropolishing and anodic oxidation on morphology, chemical composition and corrosion resistance of niobium. *Mater Sci Eng, C* 42:529–537
- [47] Heakal FE, Ghoneim AA, Mogoda AS, Awad K (2011) Electrochemical behaviour of Ti–6Al–4V alloy and Ti in azide and halide solutions. *Corros Sci* 53:2728–2737
- [48] Sepúlveda M, Quintero D, Castaño JG, Echeverría F (2018) Improved two-step Brytal process for electropolishing of aluminum alloys. *Corros Sci* 136:386–392

**Publisher's Note** Springer Nature remains neutral with regard to jurisdictional claims in published maps and institutional affiliations.